Behavior of a Moist Kelvin Wave Packet with Nonlinear Heating

BIN WANG AND YAN XUE

Department of Meteorology, University of Hawaii, Honolulu, Hawaii

(Manuscript received 26 July 1990, in final form 15 January 1991)

ABSTRACT

The effects of nonlinear (positive only or conditional) heating on moist Kelvin waves are examined with a simple equatorial zonal-plane model describing the gravest baroclinic mode.

The unstable perturbation subject to nonlinear heating emerges as a wave packet. A typical amplifying, eastward-moving wave packet is characterized by an asymmetric structure: 1) the ascending branch (wet region) is much narrower than the two descending ones (dry regions); and 2) the circulation cell to the east of the wet region center is smaller and stronger than its counterpart to the west of the center. The wet–dry asymmetry is primarily caused by the nonlinear heating effect, while the east–west asymmetry is a result of the movement of the wave packet relative to mean flow. The existence of Newtonian cooling and Rayleigh friction enhances the structural asymmetries.

The unstable wave packet is characterized by two zonal length scales: the ascending branch length (ABL) and total circulation extent (TCE). For a given basic state, the growth rate of a wave packet increases with decreasing ABL or TCE. However, up to a moderate growth rate (order of day^{-1}) the energy spectra of all wave packets are dominated by zonal wavenumber one regardless of ABL size. In particular, the slowly growing (low frequency) wave packets normally exhibit TCEs of planetary scale and ABLs of synoptic scale.

Observed equatorial intraseasonal disturbances often display a narrow convection region in between two much broader dry regions and a total circulation of planetary scale. These structure and scale characteristics are caused by the effects of nonlinear heating and the cyclic geometry of the equator. It is argued that the unstable disturbance found in numerical experiments (e.g., Lau and Peng; Hayashi and Sumi) is a manifestation of the nonlinear wave packet.

1. Introduction

Observed eastward-moving Madden–Julian (40–50 day) waves often display a synoptic-scale ascending (convection) region in between two much larger descending (dry) regions. The circulation anomalies associated with the ascending and descending areas form a coherent planetary-scale circulation cell (e.g., Madden and Julian 1972; Knutson and Weickmann 1987; or Figs. 2 and 3 of Rui and Wang 1990). This feature appears to be reproducible in numerical simulations using general circulation models or simple numerical models (e.g., Hayashi and Sumi 1986; Lau and Peng 1987; Hendon 1988; Lau et al. 1988; Swinbank et al. 1988; Hayashi and Golder 1988).

Efforts have been made to explain why the Madden–Julian waves have a characteristic planetary zonal circulation scale. The inviscid linear instabilities resulting from condensation–moisture convergence feedback (wave-CISK) (e.g., Hayashi 1970; Lindzen 1974; Chang and Lim 1988) or the evaporation–wind feedback (Neelin et al. 1987; Emanuel 1987) all failed to explain the selection of planetary-scale motion due to explosive growth of short waves. Although the heating associated with boundary-layer moisture convergence was shown to be able to integrate vertical modes and/or horizontal modes (long Kelvin and Rossby waves) such that the generation of wave energy maximizes at planetary scales (Wang and Chen 1989; Wang and Rui 1990), the linear theory does not explain the cause of the observed asymmetries in size and strength between the ascending and descending branches.

In their numerical experiments, Lau and Peng (1987, hereafter denoted as LP) found that with positive-only heating (also referred to as conditional heating or nonlinear heating; i.e., the heat is released only in large-scale ascending areas) the disturbances take on a wavenumber-one structure with most of their energy in the longest wavelength component. Recently, Lim et al. (1990) argued that the nonlinearity associated with the positive-only heating operates effectively even for an infinitesimal perturbation. In this sense, the CISK mechanism inherently possesses a severe form of nonlinearity. They solved an initial-value problem with a simple two-dimensional spectral model and demonstrated that the nonlinear heating is able to produce exponentially growing, large-scale flow patterns that propagate eastward without change of shape. Using controlled numerical experiments, Itoh (1989) found that in order for a super cloud cluster to dominate

Corresponding author address: Dr. Bin Wang, University of Hawaii, Department of Meteorology, 2525 Correa Rd, HIG 331, Honolulu, HI 96822.

among other possibly growing clusters, dry regions must be assumed to exist over wide areas in which the generation of cumulus by weak moisture convergence is artificially prohibited. This mechanism of suppressing small-scale cumulus is similar to an enhanced positive-only heating.

The positive-only heating parameterization has been adopted in the previous studies of Ekman–CISK (Charney and Eliassen 1964; Syono and Yamasaki 1966; Koss 1975). The pioneering study of Ekman–CISK with positive-only heating (Charney and Eliassen 1964) showed that the fastest growing mode exhibits a mesoscale (50 km) ascending region (the radius of ascending region was defined as a characteristic scale for the Ekman–CISK disturbance). The question thus arises: does the positive-only heating have different impact on the scale dependence of growth rate for equatorial Kelvin wave–CISK and the Ekman–CISK? Furthermore, is the asymmetric nature of the nonlinear heating responsible for the structural asymmetry between the wet (ascending) and dry (descending) regions? In a more general perspective, what are the effects of positive-only heating on the equatorial wave dynamics?

In this study we address these questions in terms of the simplest model of equatorial Kelvin wave–CISK that depicts only the gravest baroclinic mode. Rigorously speaking, the presence of convective heating does not allow a pure zonal motion since thermally forced overturning always induces significant off-equatorial meridional flows. Such an idealized model is merely instrumental in demonstrating the wave–CISK mechanism and has been widely employed in theoretical analysis (e.g., Emanuel 1987; Neelin et al. 1987; Lau and Peng 1987; Wang 1988). The solutions may be viewed as the lowest-order approximations to those of more complete two-dimensional models. A description of the model is given in section 2. The simplicity of this model allows us to derive an analytical solution in section 3 by solving two linear problems in wet and dry regions separately and then matching solutions at the wet–dry boundaries, following Charney and Eliassen (1964). It is demonstrated in sections 4 and 5 that the behavior of the unstable mode in the present model shares similarities with the unstable disturbances found in numerical studies of an initial-value problem of Kelvin wave–CISK such as LP and Lim et al. (1989). The analytical solution helps to reveal a number of distinct features of this nonlinear mode. It enables us to better understand why the slowly growing mode often displays a planetary-scale circulation cell with a synoptic-scale ascending branch.

2. The model

To focus on the effect of the positive-only heating and to make the problem analytically tractable, we consider small-amplitude motion about an uniform basic state that moves with a constant zonal speed U_0. Since diabatic heating with a maximum in the middle troposphere primarily stimulates the gravest baroclinic mode, a single vertical mode is considered (Gill 1980). The moist equatorial Kelvin wave can be investigated on an equatorial β plane with pressure coordinates by neglecting meridional motion; that is,

$$\frac{\partial u}{\partial t} + U_0 \frac{\partial u}{\partial x} + \frac{\partial \phi}{\partial x} = 0, \tag{2.1a}$$

$$\beta y u + \frac{\partial \phi}{\partial y} = 0, \tag{2.1b}$$

$$\frac{\partial \phi}{\partial t} + U_0 \frac{\partial \phi}{\partial x} + C_0^2 \frac{\partial u}{\partial x} = -\frac{R}{2C_p} Q_2, \tag{2.1c}$$

where u and ϕ can be interpreted as perturbational zonal velocity and geopotential of the lower layer of the atmosphere. Here $C_0 = (S_2 \Delta p^2/2)^{1/2}$ is the long gravity-wave speed of the gravest baroclinic mode, S_2 is the static stability parameter at $p_2 = 500$ mb, and $\Delta p = p_2$. In (2.1c), R and C_p are the gas constant for air and the specific heat at constant pressure, and Q_2 denotes the total diabatic heating rate per unit mass at p_2. For simplicity, Q_2 only contains parameterized convective latent heat and Newtonian cooling, that is,

$$Q_2 = -\delta L_c q_0 \frac{\partial u}{\partial x} + \mu \frac{2C_p}{R} \phi, \tag{2.2a}$$

where L_c is the latent heat, q_0 represents the mean specific humidity of the basic state in the lower layer (the upper layer is assumed to be dry), μ is a constant coefficient for Newtonian cooling, and

$$\delta = \begin{cases} 1, & \text{if } \partial u/\partial x < 0 \\ 0, & \text{if } \partial u/\partial x > 0. \end{cases} \tag{2.2b}$$

The convective heating term in (2.2a) is related to moisture convergence in a simple nonlinear fashion: in a region of low-level moisture convergence the extra moisture gained by convergence is condensed out, releasing latent heat, whereas in a region of moisture divergence no latent heat is released.

The diagnostic Eq. (2.1b) implies a geostrophic balance between the zonal wind and geopotential. It can be shown from linear analyses that this constraint is necessary in determining the meridional wave structure and direction of wave propagation, and it does not affect the instability and zonal structure. The success of a 2D (equatorial zonal plane) model in reproducing 3D model results (Lim et al. 1989) leads us to believe that the essence of the instability with nonlinear heating can be captured by a 2D model. To facilitate mathematical analysis, we will confine our analysis to motions on the equatorial zonal plane. The nondimensional equations can be simplified as

$$\frac{\partial u}{\partial t} + U_0 \frac{\partial u}{\partial x} + \frac{\partial \phi}{\partial x} = 0, \quad (2.3a)$$

$$\frac{\partial \phi}{\partial t} + U_0 \frac{\partial \phi}{\partial x} + N\phi + (1 - \delta I) \frac{\partial u}{\partial x} = 0, \quad (2.3b)$$

where

$$N = \mu/(\beta C_0)^{1/2}, \quad (2.4a)$$

$$I = q_0(RL_c/2C_pC_0^2). \quad (2.4b)$$

In Eqs. (2.3a, b), we have used the length scale $(C_0/\beta)^{1/2}$, the time scale $(\beta C_0)^{-1/2}$, the horizontal velocity scale C_0, and the geopotential scale C_0^2. With $\Delta P(\beta C_0)^{1/2}$ being vertical p-velocity scale, the continuity equation gives $\omega_2 = \partial u/\partial x$. The nondimensional numbers I and N measure the heating intensity or the basic-state moisture content in the lower layer and the strength of Newtonian cooling, respectively. It is obvious that the heating simply acts to reduce the static stability in the model describing the gravest baroclinic mode.

3. The nonlinear mode solution

In either the wet or dry region alone, Eqs. (2.3a, b) depict a zonally propagating Kelvin wave. The nonlinear heating, however, can unify the wave motions in the two regions to form a nonlinear mode with a constant speed propagating through the entire domain without change of shape, as demonstrated by the numerical experiments (LP; Lim et al. 1989). Let us assume, without loss of generality, that Eqs. (2.3a, b) allow a nonlinear mode solution that propagates zonally at a speed c.

To facilitate analysis, we introduce a new coordinate moving at the propagation speed c, that is,

$$x_* = x - ct. \quad (3.1)$$

The governing equations (2.3a,b) in the moving coordinates become

$$\frac{\partial u_*}{\partial t} + U_* \frac{\partial u_*}{\partial x_*} + \frac{\partial \phi_*}{\partial x_*} = 0, \quad (3.2a)$$

$$\left(\frac{\partial}{\partial t} + N\right)\phi_* + U_* \frac{\partial \phi_*}{\partial x_*} + (1 - \delta I) \frac{\partial u_*}{\partial x_*} = 0, \quad (3.2b)$$

where

$$U_* = U_0 - c \quad (3.3)$$

represents the mean flow speed relative to the moving disturbances (hereafter referred to as relative mean zonal flow), and u_* and ϕ_* are functions of x_* and t. Eliminating ϕ_* between (3.2a) and (3.2b) leads to

$$\frac{\partial^2 u_*}{\partial t^2} + 2U_* \frac{\partial^2 u_*}{\partial t \partial x_*} - (1 - \delta I - U_*^2) \frac{\partial^2 u_*}{\partial x_*^2} + N\left(\frac{\partial u_*}{\partial t} + U_* \frac{\partial u_*}{\partial x_*}\right) = 0. \quad (3.4a)$$

Knowing u_*, ϕ_* and ω_* can be obtained from

$$\left(\frac{\partial}{\partial t} + N\right)\phi_* = U_* \frac{\partial u_*}{\partial t} - (1 - U_*^2 - \delta I) \frac{\partial u_*}{\partial x_*}, \quad (3.4b)$$

and

$$\omega_* = \partial u_*/\partial x_*. \quad (3.4c)$$

Since in the transformed coordinates the unstable modes become stationary, it is natural to assume nonlinear mode solutions of Eqs. (3.4a, b, c) with the form

$$(u_*, \phi_*, \omega_*) = e^{\sigma t}(U(x_*), \Phi(x_*), W(x_*)) \quad (3.5)$$

where U, Φ, W are, respectively, the zonal structure functions of zonal wind, geopotential height, and vertical p-velocity fields, and σ is the growth rate. Substituting (3.5) into (3.4a) yields

$$(U_*^2 - 1 + \delta I)U'' + (2\sigma + N)U_* U' + \sigma(N + \sigma)U = 0, \quad (3.6)$$

where the prime denotes derivative wrt x_*.

Although (3.6) is nonlinear in the entire domain, it is linear within the "wet" or "dry" region alone. In what follows, the subscripts w and d are used to distinguish quantities in the wet and dry regions, respectively. Thus, U_w and U_d satisfy, respectively,

$$(U_*^2 - 1 + I)U_w'' + (2\sigma + N)U_* U_w' + \sigma(N + \sigma)U_w = 0, \quad (3.7a)$$

$$(U_*^2 - 1)U_d'' + (2\sigma + N)U_* U_d' + \sigma(N + \sigma)U_d = 0, \quad (3.7b)$$

which have the following general solutions:

$$U_w(x_*) = \exp(m_w x_*) \times [A_1 \exp(n_w x_*) + A_2 \exp(-n_w x_*)], \quad (3.8a)$$

$$U_d(x_*) = \exp(m_d x_*) \times [B_1 \exp(n_d x_*) + B_2 \exp(-n_d x_*)], \quad (3.8b)$$

with

$$m_w = -U_*(N + 2\sigma)/[2(U_*^2 - 1 + I)], \quad (3.9a)$$

$$n_w = \sqrt{N^2 U_*^2 + 4\sigma(N + \sigma)(1 - I)}/[2(U_*^2 - 1 + I)], \quad (3.9b)$$

$$m_d = -U_*(N + 2\sigma)/[2(U_*^2 - 1)], \quad (3.9c)$$

$$n_d = \sqrt{N^2U_*^2 + 4\sigma(N + \sigma)}/[2(U_*^2 - 1)]. \quad (3.9d)$$

The determination of the growth rate and structure of a nonlinear mode requires matching of linear solutions at the internal boundaries between the wet and dry regions. The geometry of the zonal domain and the boundary locations are illustrated in Fig. 1. The domain size is limited by the full span of the equator, which, in nondimensional form, is

$$L = 2\pi R_a(\beta/C_0)^{1/2},$$

where R_a is the radius of the earth. It is convenient to set the origin ($x_* = 0$) at the center of the wet region where zonal velocity vanishes, that is,

$$U_w(0) = 0. \quad (3.10a)$$

To the east (west) of the origin the low-level wind is easterly (westerly). Continuity requires that another point must exist where the zonal wind also vanishes in the dry region. It is convenient for us to take this point as the boundary where periodic boundary conditions apply. However, the location of this point [i.e., the fetch of the low-level easterly (westerly) wind] is unknown a priori. Without loss of generality, the domain boundaries are set at $-\gamma s$ and s, respectively, where $s = L/(1 + \gamma)$ and γ is the ratio of the length scale of the circulation cell west of the wet region center (westerlies) to that east of the center (easterlies), which measures the asymmetry of the circulation relative to the origin over the entire domain. At the domain boundaries, $x_* = s$ and $-\gamma s$, the perturbation zonal velocity and its first derivative wrt x_* satisfy the continuity conditions, that is,

$$U_{d+}(s) = U_{d-}(-\gamma s) = 0, \quad (3.10b)$$

and

$$U'_{d+}(s) = U'_{d-}(-\gamma s), \quad (3.10c)$$

where the plus and minus subscripts denote solutions in the right and left dry region, respectively (see Fig. 1).

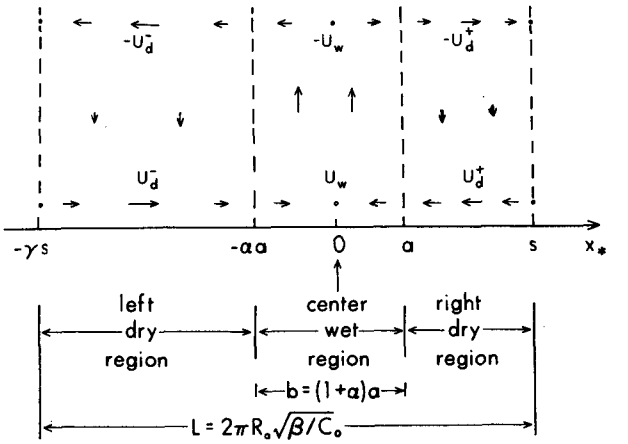

FIG. 1. The geometry of the model domain and the sketch of the perturbation motion in the model. Symbols are explained in the text.

Likewise, the left and right internal boundaries between the wet and dry regions can be represented by $-\alpha a$ and a, respectively. The total length of the wet region (or ascending branch) is $b = (1 + \alpha)a$, where α is a measure of the asymmetry of the circulation within the wet region. Across the internal boundaries, $x_* = a$ and $-\alpha a$, the mass and pressure must be continuous. This will be warranted by the following matching conditions:

$$U_w(a) = U_{d+}(a), \quad (3.10d)$$

$$U_w(-\alpha a) = U_{d-}(-\alpha a), \quad (3.10e)$$

$$(U_*^2 + I - 1)U'_w(a) = (U_*^2 - 1)U'_{d+}(a), \quad (3.10f)$$

$$(U_*^2 + I - 1)U'_w(-\alpha a) = (U_*^2 - 1)U'_{d-}(-\alpha a). \quad (3.10g)$$

With the aid of Eq. (3.10a), the wet region solution (3.8a) becomes

$$U_w(x_*) = A \exp(m_w x_*) sh(n_w x_*), \quad -\alpha a \leq x_* \leq a. \quad (3.11a)$$

Similarly, with constraints (3.10b) and (3.10c), the dry region solution (3.8b) becomes

$$U_d(x_*) = \begin{cases} U_{d+}(x_*) = B \exp(m_d x_*) shn_d(s - x_*), & a \leq x_* \leq s \\ U_{d-}(x_*) = -B \exp[m_d(1 + \gamma)s] \exp(m_d x_*) shn_d(\gamma s + x_*), & -\gamma s \leq x_* \leq -\alpha a. \end{cases} \quad (3.11b)$$

Substitution of (3.11a, b) into the matching conditions (3.10d, e, f, g) yields

$$B = A \exp[(m_w - m_d)a] shn_w a / shn_d(s - a), \quad (3.11c)$$

and

$$shn_d(s - a) shn_w \alpha a = \exp[(m_w - m_d)(1 + \alpha)a + m_d(1 + \gamma)s] shn_d(\gamma s - \alpha a) shn_w a, \quad (3.12)$$

$$(U_*^2 + I - 1)n_w thn_d(s - a) = -(U_*^2 - 1)n_d thn_w a, \quad (3.13)$$

$$(U_*^2 + I - 1)n_w thn_d(\gamma s - \alpha a) = -(U_*^2 - 1)n_d th\alpha n_w a. \quad (3.14)$$

Equations (3.12), (3.13), and (3.14) determine the relationships among the growth rate σ, the structural asymmetry parameters (α and γ) and zonal scale (a or b), the basic flow properties (I, U_*), and the thermal damping rate (N). This set of equations may be referred to as the dispersion relations for the nonlinear mode. Equations (3.11a, b, c) describe the structure of zonal wind field for the nonlinear mode. The corresponding structures for geopotential and vertical p velocity can be readily obtained from Eqs. (3.4b) and (3.4c).

In the absence of Newtonian cooling, the dispersion equation (3.12) remains the same, but (3.13) and (3.14) are simplified as

$$\sqrt{1-I}thn_d(s-a) = -thn_w a, \tag{3.15}$$

$$\sqrt{1-I}thn_d(\gamma s-\alpha a) = -th\alpha n_w a, \tag{3.16}$$

with parameters m_w, m_d, n_w, and n_d defined by

$$m_w = -\sigma U_*/(U_*^2 + I - 1), \tag{3.17a}$$

$$n_w = |\sigma|\sqrt{1-I}/(U_*^2 + I - 1), \tag{3.17b}$$

$$m_d = -\sigma U_*/(U_*^2 - 1), \tag{3.17c}$$

$$n_d = |\sigma|/(U_*^2 - 1). \tag{3.17d}$$

It is worthwhile to make a few remarks on the nonlinear solutions (3.11a, b) before showing the numerical results.

1) A meaningful solution obtained with the proposed boundary and matching conditions requires that the vertical velocity does not change its sign within the wet (or dry) region and the zonal velocity has the same sign either ahead of or behind the wet region center. It can be shown that the solutions (3.11a, b) always satisfy these requirements.

2) It can be proven that if the nonlinear heating is replaced by linear heating the results in this section match the linear theory. In fact, with $\delta = 1$ over the entire domain and using the periodic boundary conditions, the general solution (3.8a) reduces to a linear normal-mode structure (sinusoidal wave) with growth rate and phase speed satisfying the linear dispersion relation. Determination of the direction of phase propagation and the meridional structure requires further use of meridional boundary conditions.

3) It can be shown that the growth rate does not change when the relative mean zonal flow reverses its direction. However, the zonal structure of the perturbation in a relative mean westerly flow is a mirror image of that in a relative mean easterly flow with respect to the wet region center; namely, the circulation cell to the east of the wet region center is larger and weaker than its counterpart to the west of the center. In both cases, the circulation cell is reinforced and compressed in the "windward" side.

4) There exists a threshold heating intensity (or moisture content) I_c for the instability, which is

$$I_c = 1 - U_*^2. \tag{3.18}$$

If $I \leqslant I_c$, only neutral modes are possible, while unstable modes emerge when $I > I_c$. In the absence of mean flow, (3.18) matches the linear theory. With nonlinear heating the instability threshold is affected by the propagation speed relative to the mean flow.

5) The existence of unstable modes requires that

$$|U_*| = |U_0 - c| < 1. \tag{3.19}$$

If there were no mean flow, the constraint (3.19) would imply that the propagation speed of the moist unstable mode could not exceed the long gravity wave speed in dry atmosphere. This agrees with our experience in dealing with linear waves: an addition of latent heating always slows down wave propagation.

4. The behavior of unstable nonlinear modes

The analytical solutions provide an opportunity for close scrutiny and better understanding of the dynamics of the unstable nonlinear mode. The basic nondimensional parameters in the present model are I, N, and U_*. Their meanings are briefly explained in Table 1. We note that the relative mean flow U_* denotes the mean zonal flow observed following the moving perturbation. For a stationary mode U_* simply represents the mean flow speed, while in a quiescent basic state U_* equals $-c$ (c is phase speed). In what follows, except as otherwise stated, the following values are used for the basic model parameters: $I = 1.15$, $U_* = -0.2$, and $N = 0.0$.

a. The growth rate

It is convenient to define the ascending branch length (ABL) as a characteristic scale of the unstable mode. The dependence of growth rate on ABL is illustrated in Fig. 2 for a number of parameter settings. In all cases the most striking feature is that the growth rate unboundedly increases as the ABL decreases. Thus, for a fixed basic-state parameter setting, the fastest

TABLE 1. The basic model parameters.

β	Equatorial β parameter ($\beta = 2\Omega/a$)	2.3×10^{-11} m^{-1} s^{-1}
C_0	Long gravity-wave speed of the gravest baroclinic mode	50 m s^{-1}
q_0	Mean specific humidity in the lower layer between 500 and 1000 mb	8.0 g kg^{-1}
μ	Newtonian cooling coefficient	5×10^{-6} s^{-1}
U_*	Nondimensional basic zonal flow velocity relative to propagating wave packet	−0.20
N	Nondimensional Newtonian cooling coefficient	0.25
I	Nondimensional measurement of the mean moisture content in the lower layer	1.15

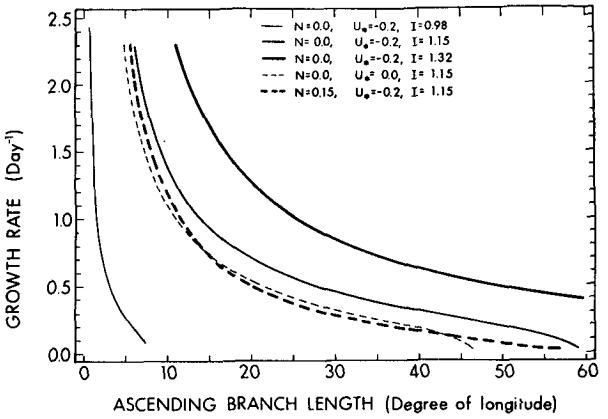

FIG. 2. Growth rate of the nonlinear mode as a function of the ascending branch length for different heating intensity (I), Newtonian cooling rate (N), and relative zonal mean flow (U_*).

growing mode has the smallest ABL. In the numerical experiment of Lim et al. (1989), the disturbance with a narrower convection and circulation region indeed grew faster. The ABL of the fastest growing disturbance is comparable to the resolvable scale of their spectral model. The present results suggest that without the limitation of the model resolution, the ABL of the fast growing mode possibly assumes even smaller scale. Similar behavior was previously found in Ekman–CISK with nonlinear heating (e.g., Charney and Eliassen 1964). It seems that the effect of positive-only heating on the dependence of growth rate on the scale of the ascending branch is similar in Ekman–CISK and Kelvin wave–CISK. In both cases, the smaller the ascending region is, the faster the unstable mode grows.

Comparison of the three solid curves in Fig. 2 indicates that the growth rate of unstable modes increases with increased moisture content or heating intensity. This behavior resembles that of the linear normal mode. It is, however, interesting to observe the influence of the relative mean flow on the growth rate. The comparison of the results for cases with and without relative mean flow in Fig. 2 shows that the presence of an easterly relative mean flow reinforces the instability.

b. The zonal structure

The unstable mode subject to nonlinear heating possesses a fixed shape (structure) with amplitude growing exponentially. The structure, however, varies with the basic-state parameters and its characteristic scales. A representative zonal structure for a growing mode in a relative mean easterly flow is illustrated in Fig. 3a. The length of ascending branch is assumed to occupy about one-tenth of the equatorial belt. The most prominent structural feature is the asymmetry. Two types of asymmetry are identified. First, the ascending branch (wet region) is much narrower than the descending branches (dry regions). This wet–dry asymmetry is observed in the structure of intraseasonal oscillations. It was found by previous numerical studies of both Ekman–CISK (e.g., Syono and Yamasaki 1966; Koss 1975) and equatorial wave–CISK (LP; Lim et al. 1989). Second, the circulation to the east of the wet-region center is more intense than that to the west, while the spatial scale of the low-level easterlies is smaller than that of westerlies. This second asymmetry was reported by LP and Lim et al. (1989) for eastward-moving disturbances. For a mode stationary relative to the mean flow, the east–west asymmetry disappears (Fig. 3b). This indicates that the positive-only heating alone is not sufficient, while the presence of relative mean flow is essential for the creation of the east–west asymmetry.

The structure varies when heating intensity (I) or Newtonian cooling rate (N) changes. In response to a stronger heating intensity, the circulation and geopotential are reinforced in the vicinity of the two internal boundaries and are weakened in the dry regions far away from the internal boundaries (Fig. 3c). Meanwhile, the growth rate increases substantially. This implies that a more rapidly amplifying mode has its energy more concentrated in the vicinity of the wet region. The Newtonian cooling slightly diminishes the strength of the circulation but dramatically reduces the geopotential (Fig. 3d). As a consequence of the uneven damping between the zonal wind and geopotential, the ratio of kinetic to available potential energy of the nonlinear mode increases.

Since the structural asymmetry is a fundamental feature of the nonlinear mode, it deserves closer scrutiny. Figures 4a and 4b show how the asymmetries described by parameters α and γ vary with b (ABL) (cf. Fig. 1 for the definition of α, γ, and b) for growing nonlinear modes under different basic-state conditions. Several features are noticeable. First, there is a cutoff ABL for each given heating intensity and thermal damping. In the absence of Newtonian cooling, the cutoff ABL under a typical heating intensity ($I = 1.15$) is about 60 degrees of longitude, implying that the ascending branch covers a much smaller area than the descending branches. Increasing Newtonian cooling reduces, while increasing heating intensity increases the cutoff ABL significantly. Second, γ is generally greater than α, particularly for small ABLs. This means that the east–west asymmetry of spatial scale lies principally in the descending branches. Since γ increases with decreasing ABL the mode with a narrower wet region exhibits a larger structural asymmetry. However, the degree of the asymmetry is limited, because γ attains its maximum value of 1.5 as ABL approaches zero. Finally, the addition of Newtonian cooling enhances the structural asymmetry, especially for the modes with large ABL.

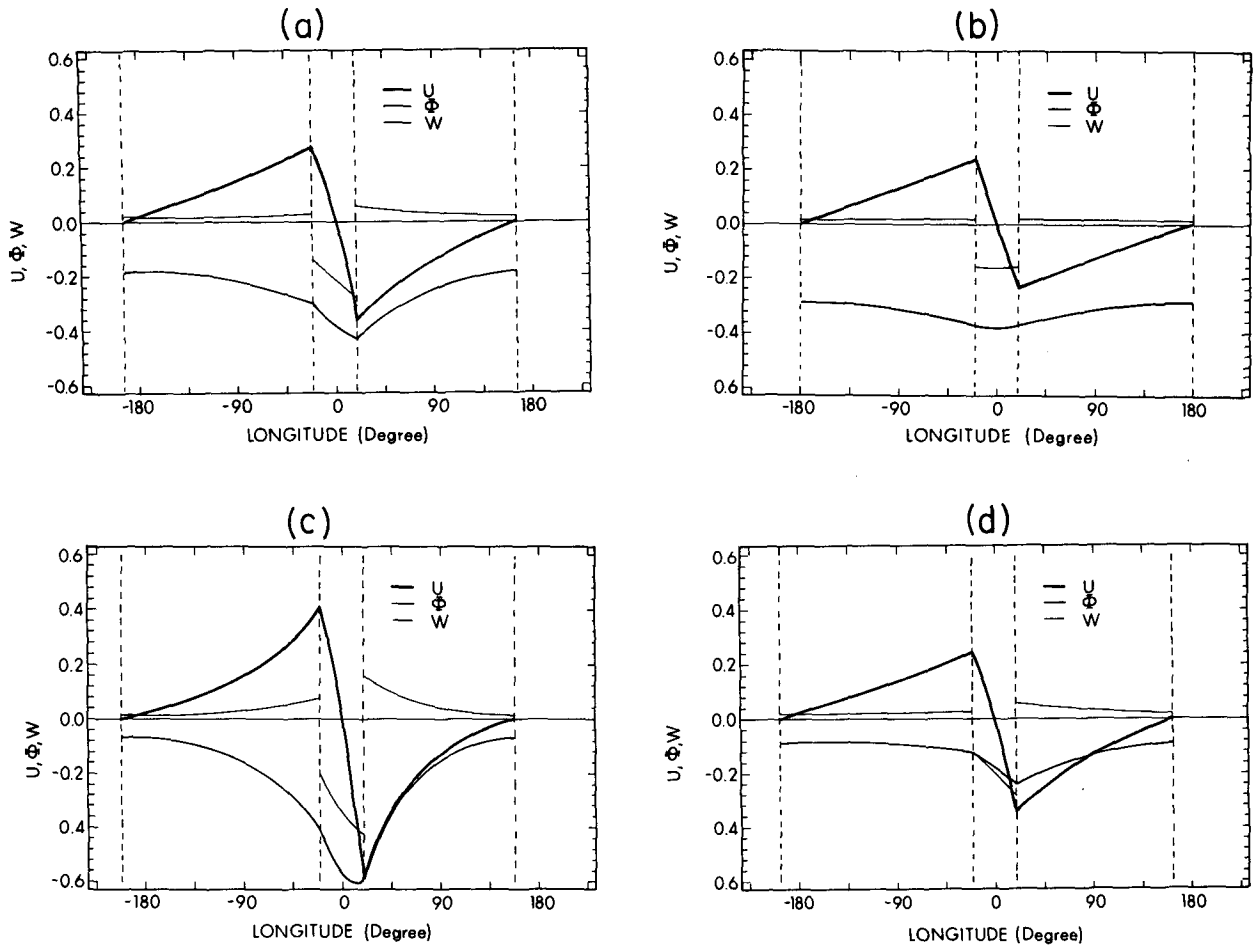

FIG. 3. Structure of the zonal wind, geopotential height, and vertical pressure velocity for nonlinear modes computed using the following parameter values: (a) $I = 1.15$, $U_* = -0.2$, and $N = 0.0$; (b) $I = 1.15$, $U_* = 0.0$, and $N = 0.0$; (c) $I = 1.32$, $U_* = -0.2$, and $N = 0.0$; and (d) $I = 1.15$, $U_* = -0.2$, and $N = 0.15$. The ascending branch length is 40 degrees of longitude.

c. *The effects of dissipation*

With linear heating Newtonian cooling dissipates disturbances nearly equally for all wavelengths. With nonlinear heating the dissipation effect of the Newtonian cooling is weakly scale dependent. Although it severely affects large scales, the amount of growth rate reduced by Newtonian cooling rate N is nearly a constant (slightly smaller than $N/2$) for perturbations with ABL smaller than 30 degrees of longitude. This, as a matter of fact, is reminiscent of the effect in the linear case (Wang 1988). As a consequence, the weakly unstable modes whose inviscid growth rate is comparable to the magnitude of the Newtonian cooling rate will be crucially affected.

Other forms of dissipation have also been tested in the framework of the present model. Without developing formula, we simply state the results.

1) If a Rayleigh friction alone is added to the zonal momentum equation, it plays an equivalent role as Newtonian cooling in reducing the growth rate. Yet, Rayleigh friction does not damp the geopotential field as remarkably as Newtonian cooling does.

2) A combination of Newtonian cooling and Rayleigh friction with an equal damping rate will reduce the growth rate for all scales (ABL) by an amount equal to the sum of the damping rate due to the Newtonian cooling and Rayleigh friction alone.

3) If both dissipation mechanisms coexist and have different strengths, τ_1^{-1} and τ_2^{-1} ($\tau_1^{-1} > \tau_2^{-1}$), the growth rate would be reduced by τ_2^{-1} plus a reduction caused by a Newtonian cooling (or Rayleigh friction) alone with a strength ($\tau_1^{-1} - \tau_2^{-1}$).

The effects of dissipation on the growth rate bear similarities to their counterparts in a linear heating case. That is, the dissipation effects do not seem to be influenced by the nonlinear heating. However, the presence of Newtonian cooling and Rayleigh friction enhances the structural asymmetries of the nonlinear mode.

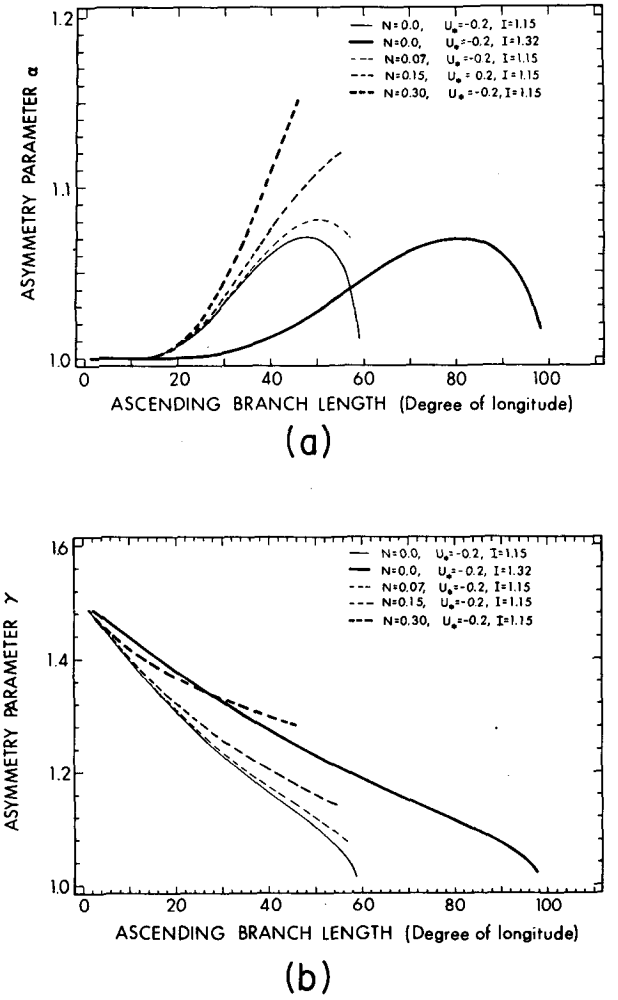

FIG. 4. (a) Asymmetry parameter α (the ratio of the zonal scale of the low-level westerlies to that of the easterlies in the wet region) as a function of ascending branch length. (b) The same as (a) except for parameter γ, which denotes the ratio of the zonal scale of the low-level westerlies to that of the easterlies over the entire domain. Parameter values used to compute each curve are given in the legends.

d. *The influence of zonal boundary conditions*

The choice of a periodic boundary condition is physically consistent with the cyclic nature of the equatorial geometry. The energy of the resultant unstable mode is concentrated in a relatively small region, especially when the growth rate is large. For those fast growing modes, their behavior might not be severely distorted if the periodic boundary condition were replaced by an infinite boundary condition that requires that perturbation fields vanish at infinity. Solutions with such a boundary condition can be derived with much less mathematical manipulations. Figure 5 compares the results obtained using the two different boundary conditions. For fast growing modes the growth rates are nearly the same (Fig. 5a). The corresponding structures also differ negligibly. For the slowly growing modes, however, with the infinite boundary condition the growth rate is overestimated (Fig. 5a) and the circulation cell is elongated; yet, the east–west asymmetry in the strength remains (Figs. 5b and 5c). The use of a periodic boundary condition (3.10) restrains the extent of circulation, and yields slowly growing modes. Therefore, the existence of the slowly growing mode appears to crucially depend on the cyclic nature of the zonal domain.

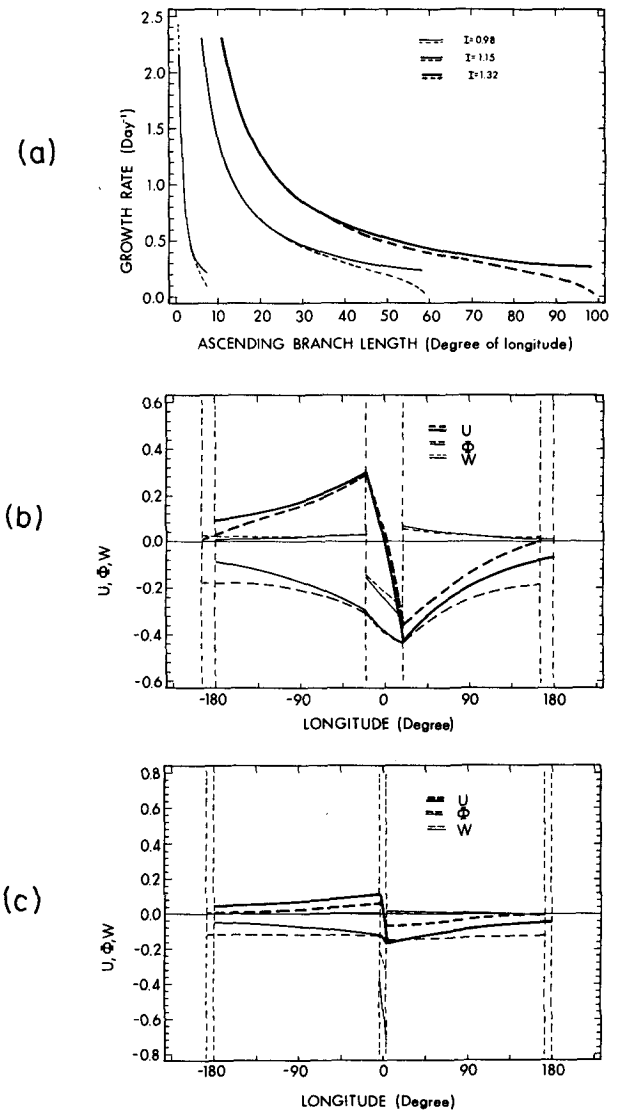

FIG. 5. (a) The growth rate and (b), (c) zonal structures of the nonlinear modes computed using the infinite boundary conditions (solid curves). For the convenience of comparison the corresponding solutions computed using periodic boundary conditions are also shown by dashed curves. The ascending branch length is 40° longitude in (b) and 7° longitude in (c).

5. Discussions and conclusions

a. Limitations of the present model

The model used in this study is the simplest model suitable for demonstration of the nonlinear heating effects on moist equatorial waves. It involves two additional simplifications compared with LP's numerical model. First, the vertical resolution was reduced from five to two levels so that only the gravest baroclinic mode is described. A drawback of the single-mode model is that the heating simply acts to reduce the basic-state static stability and the unstable Kelvin mode is stationary with an oscillatory meridional structure. When heating is distributed at multilevels, the interaction of vertical modes will yield a propagating unstable mode. The essential features of the instability, however, can be qualitatively illustrated using a two-level model. The second simplification is the neglect of meridional variation. This saves an enormous amount of mathematical manipulations, but leads to undetermined meridional structure and phase speed c. This, however, should not be regarded as a serious defect, because the behavior of the nonlinear mode in the 2D equatorial zonal plane model is qualitatively the same as that in a 3D model as demonstrated by numerical experiments (Lim et al. 1989). As a matter of fact, we have solved a problem with the v-momentum equation included using infinite horizontal boundary conditions. The resultant unstable mode is stationary and has an equatorially trapped meridional structure. The features in zonal structure and growth rate are similar to those we have obtained from the present 2D model.

b. The asymmetric zonal structure

The most salient feature of the nonlinear mode is its asymmetric structure. For a typical value of atmospheric heating intensity (or moisture content), there is an upper bound for the ABL that is about 60 degrees of longitude (Fig. 4). Thus, the zonal scale of the ascending branch is normally much smaller than that of descending branches. From mass continuity, it follows that the upward motion must be much more intense than the downward motion. This asymmetry common to both Ekman–CISK and wave–CISK is a direct consequence of the nonlinear heating. By removing physically unrealistic negative heating in the descending region, the energy can be generated only within the ascending region. As a result of the CISK selectivity in the ascending region, the length of the ascending branch tends to decrease. On the other hand, the adjacent descending branches passively respond to the lateral forcing from the ascending branch, covering a much broader domain (Chang and Lim 1988). Under normal heating intensity ($I = 1.15$) and for the slowly growing mode (growth rate $< 0.3\ \text{day}^{-1}$), only periodic boundary conditions can restrain the ascending branch length to create this wet–dry asymmetry (Fig. 5a). In this sense, the wet–dry asymmetry is partially attributed to the cyclic geometry of the equatorial belt.

In addition to the wet–dry asymmetry, there is an east–west asymmetry in the zonal structure; that is, the circulation cell to the east of the wet region center is smaller in size and stronger in strength than its counterpart to the west of the center (Fig. 3a). This asymmetry, however, is primarily caused by the propagation of the nonlinear mode relative to the mean flow. It disappears if the mode is stationary relative to the environmental flow. On the other hand, it is enhanced when the propagation speed relative to the mean flow increases.

c. The energy spectrum of the nonlinear wave packet

Unlike linear (wavelike) heating, which forces a single Fourier mode, the nonlinear heating forces all Fourier harmonics and integrates them into a wave packet. All linear normal modes within the wave packet will eventually have the same growth rate and phase speed so that the shape of the wave packet is unchanged as demonstrated by numerical integrations (Hayashi and Sumi 1986; LP; Lim et al. 1989). The energy partition among Fourier harmonics is thus fixed. It is of interest to examine the perturbation energy spectra for different nonlinear modes.

Figure 6 depicts the energy spectra for three nonlinear modes with ABL = 40, 18.6, and 5.3 degrees of longitude, respectively. All spectra attain their maxima at wavenumber one irrespective of the ABL size. However, the shorter the ABL, the more energy is carried by short waves. In addition, the kinetic energy spectrum peaks at wavenumber three for the mode with ABL = 5.3 degrees of longitude (for the other two modes,

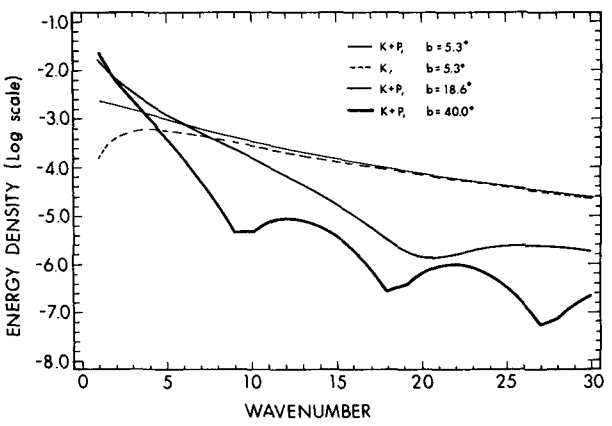

FIG. 6. The energy spectra for nonlinear wave packets with different ascending branch length b. Two hundred harmonics were used for the spectrum analysis. The solid curves are for total wave packet energy and the dashed for kinetic energy only.

the kinetic energy spectra are still dictated by wavenumber one). The mode with ABL = 18.6 degrees of longitude is similar to the disturbance simulated in LP. By decomposing the amplitude of the upper-level zonal wind into Fourier harmonics, LP concluded that when a disturbance reaches a steady state, wavenumber one contributes the most to the total zonal wind. Our results (Fig. 6) indicate that up to a moderate growth rate O(1 day^{-1}) the energy concentration on the longest wavelength is a common characteristic of nonlinear modes. It is, therefore, conceptually necessary to distinguish the dominant wavenumber in the energy spectrum from the characteristic scale of the nonlinear mode.

d. *The characteristic scales of the nonlinear wave packet*

The nonlinear mode growth rate is shown analytically to be inversely proportional to the ascending branch length (ABL), which is the width of the wet regions. In this regard, the positive-only heating has similar effect on the scale dependence of the growth rate for both Kelvin wave–CISK and traditional Ekman–CISK.

One may question the adequacy of defining the ABL as a characteristic scale for the nonlinear mode because the total circulation may cover an area much larger than the wet region. To focus on the circulation pattern one may consider another characteristic scale—the total circulation extent (TCE), which can be defined by the zonal distance between the two cutoff points where the zonal wind speed drops below one-tenth (or *e*-folding) of its maximum value at the internal boundaries.

It has been shown that the ratios of TCE to ABL for various heating intensities all approach certain finite constants as the ABL approaches zero (Fig. 7), implying that the TCE also tends to vanish. Thus, the conclusion that the smallest-scale nonlinear mode corresponds to the largest growth rate is valid regardless of which characteristic scale is considered.

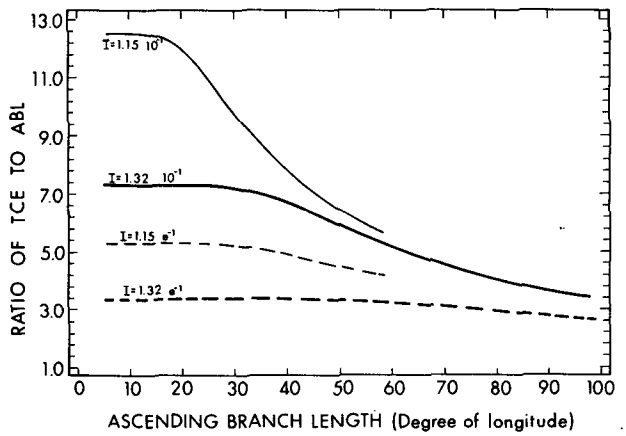

FIG. 7. The ratio of the total circulation extent (TCE) to the ascending branch length (ABL) as a function of ABL.

The TCE, on the other hand, does serve as a characteristic scale that is to some degree independent of the ABL. Figure 8a depicts the TCE as a function of the ABL for different heating intensities. As the ABL equals 5 degrees of longitude, the TCE is about 60 degrees of longitude for $I = 1.15$ if 0.1 times the maximum value is the cutoff criterion. The TCE rapidly increases with increasing ABL. As ABL reaches 25 degrees of longitude, the TCE covers 270 degrees of longitude. It is important to notice that the TCE increases with a decreasing I (or growth rate) if the ABL is fixed. This implies that for slowly growing modes, the ratio of TCE to ABL tends to be large. Figure 8b illustrates this behavior more clearly. For fast growing modes, the total circulation extent shrinks rapidly. On the other hand, for slowly growing modes (e.g., *e*-folding time greater than 5 days) the total circulation covers at least three quarters of the equator, even for the mode with an ABL as small as 5.3 degrees of longitude. This reveals an important feature of the low-frequency mode: the TCE tends to be planetary scale while the ABL is synoptic or subsynoptic scale. Therefore, the low-frequency unstable wave packet induced by nonlinear heating is characterized by two scales: the ABL and the TCE.

e. *In relation to the numerical experiment results*

Numerical integration of the initial-value problems shows that the evolution of unstable disturbances has two stages: an initial adjustment and a steady stage. In the adjustment stage, nonlinear heating induces energy transfer from short to long wavelength. The resultant wave packet has an energy spectrum dominated by wavenumber one (LP; Lau et al. 1989). In the later steady stage, this wave packet organized by nonlinear heating grows slowly without change of its shape, implying that all linear modes in the wave packet obtain identical growth rates and phase speeds (Lim et al. 1990).

The wave packet is characterized by a narrow precipitation region of synoptic scale ($\sim 10^3$ km) and a wide circulation extent of planetary scale ($\sim 10^4$ km). This double scale characteristic and asymmetric zonal structure are in good agreement with those of the nonlinear mode obtained in the present analytical model analysis. Therefore, the steady disturbance found in the numerical experiments may be viewed as a realization of one of the nonlinear wave packets.

Our results also suggest that a variety of wave packets may possibly form due to the nonlinear heating effects. They may exhibit different characteristic scales (ABL and TCE), growth rate, and structures, depending upon the nature of the initial forcing, basic flow properties,

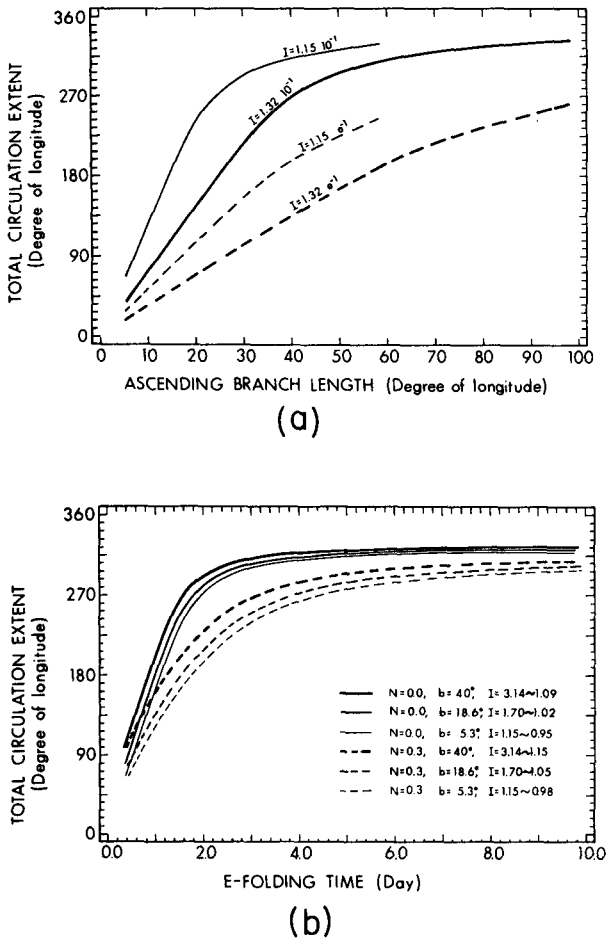

FIG. 8. The dependence of the total circulation extent on (a) ABL and (b) *e*-folding time for growing nonlinear wave packets.

and dissipation. However, up to a moderate growth rate of O(1 day^{-1}) the energy spectra of all wave packets are dominated by the lowest few wavenumbers. If the basic-state parameters and initial forcing are so constrained that the wave packet grows slowly, the total circulation extent is normally global scale, yet the ascending branch is synoptic scale. These structure and scale characteristics result from the effects of nonlinear heating and the cyclic geometry of the equator.

Acknowledgments. The authors are grateful to R. T. Pierrehumbert for suggesting that the Introduction be shortened, T. A. Schroeder for reading the manuscript, and Louis Oda for making the graphics. Support for this work was provided by National Science Foundation under Grant ATM-8814626 and NOAA/EPOCS Grant NA-85-ABH-00032, and ONR Grant N00014-90-J-1383.

REFERENCES

Chang, C.-P., and H. Lim, 1988: Kelvin wave-CISK: A possible mechanism for the 30–50 day oscillation. *J. Atmos. Sci.*, **45**, 1709–1720.

Charney, J. G., and A. Eliassen, 1964: On the growth of the hurricane depression. *J. Atmos. Sci.*, **21**, 68–75.

Emanuel, K. A., 1987: An air–sea interaction model of intraseasonal oscillation in the tropics. *J. Atmos. Sci.*, **44**, 2324–2340.

Gill, A. E., 1980: Some simple solutions of heat-induced tropical circulation. *Quart. J. Roy. Meteor. Soc.*, **106**, 447–462.

Hayashi, Y., 1970: A theory of large-scale equatorial waves generated by condensation heat and accelerating the zonal wind. *J. Meteor. Soc. Japan*, **48**, 140–160.

——, and D. G. Golder, 1988: Tropical intraseasonal oscillation appearing in a GFDL general circulation model and FGGE data. Part II: Structure. *J. Atmos. Sci.*, **45**, 3017–3033.

Hayashi, Y. Y., and A. Sumi, 1986: The 30–40 day oscillations simulated in an "Aqua Planet" model. *J. Meteor. Soc. Japan*, **64**, 451–467.

Hendon, H. H., 1988: A simple model of the 40–50 day oscillation. *J. Atmos. Sci.*, **45**, 569–584.

Itoh, H., 1989: The mechanism for the scale selection of tropical intraseasonal oscillations. *J. Atmos. Sci.*, **46**, 1779–1798.

Knutson, T. R., and K. M. Weickmann, 1987: 30–60 day atmospheric oscillation: Composite life cycles of convection and circulation anomalies. *Mon. Wea. Rev.*, **115**, 1407–1436.

Koss, W. J., 1975: Linear stability analysis of CISK-induced low latitude disturbances. NOAA Tech. Memo. ERL WMPO-24, 176 pp. [NTIS No. PB248 450].

Lau, K.-M., and L. Peng, 1987: Origin of the low frequency (intraseasonal) oscillation in the tropical atmosphere. Part I: Basic theory. *J. Atmos. Sci.*, **44**, 950–972.

——, ——, C. H. Sui, and T. Nakazawa, 1989: Dynamics of super cloud clusters, westerly wind bursts, 30–60 day oscillations and ENSO: An unified view. *J. Meteor. Soc. Japan*, **67**, 205–219.

Lau, N.-C., I. M. Held, and J. D. Neelin, 1988: The Madden-Julian oscillation in an idealized GCM model. *J. Atmos. Sci.*, **45**, 3810–3832.

Lim, H., T.-K. Lim, and C.-P. Chang, 1990: Reexamination of wave-CISK theory: Existence and properties of nonlinear wave-CISK modes. *J. Atmos. Sci.*, **47**, 3078–3091.

Lindzen, R., 1974: Wave-CISK in the tropics. *J. Atmos. Sci.*, **31**, 156–179.

Madden, R. A., and P. R. Julian, 1972: Description of global-scale circulation cell in the tropics with a 40–50 day period. *J. Atmos. Sci.*, **29**, 1109–1123.

Neelin, J. D., I. M. Held, and H. Cook, 1987: Evaporation-wind feedback and low-frequency variability in the tropical atmosphere. *J. Atmos. Sci.*, **44**, 2341–2348.

Rui, H., and B. Wang, 1990: Development characteristics and dynamic structure of tropical intraseasonal convective anomalies. *J. Atmos. Sci.*, **47**, 357–379.

Swinbank, R., T. N. Palmer, and M. K. Davey, 1988: Numerical simulation of the Madden and Julian oscillation. *J. Atmos. Sci.*, **45**, 774–788.

Syono, S., and M. Yamasaki, 1966: Stability of symmetrical motions driven by latent heat release by cumulus convection under the existence of surface friction. *J. Meteor. Soc. Japan*, **44**, 353–375.

Wang, B., 1988: Dynamics of tropical low-frequency waves: An analysis of the moist Kelvin wave. *J. Atmos. Sci.*, **45**, 2051–2065.

——, and J.-K. Chen, 1989: On the zonal scale selection and vertical structure of the equatorial intraseasonal waves. *Quart. J. Roy. Meteor. Soc.*, **115**, 1301–1323.

——, and H. Rui, 1990: The Dynamics of the coupled moist Kelvin–Rossby wave on an equatorial beta-plane. *J. Atmos. Sci.*, **47**, 397–413.